THE JOURNAL OF PHYSICAL CHEMISTRY B

Article

pubs.acs.org/JPCB

# Mapping Single Molecular Binding Kinetics of Carbohydrate-Binding Module with Crystalline Cellulose by Atomic Force Microscopy Recognition Imaging

Mengmeng Zhang,[†] Bin Wang,[†] and Bingqian Xu*,[†]

[†]Single Molecule Study Laboratory, College of Engineering and Nanoscale Science and Engineering Center, University of Georgia, Athens, Georgia 30602, United States

Supporting Information

**ABSTRACT:** We studied the binding kinetics of family 3 carbohydrate-binding module (CBM3a) molecules to crystalline cellulose fibrils extracted from the poplar cell wall by atomic force microscopy (AFM) recognition imaging. The free CBM3a molecules of different concentrations were added to the buffer solution to bind to the crystalline cellulose sample immobilized on the AFM substrate. During *in-situ* AFM imaging, the CBM molecules were observed to bind to cellulose efficiently and regularly, especially in the first 60−120 min. A 1:1 single-molecule binding model was used to study the kinetics of the CBM3a−cellulose interaction. The saturation time when the concentration of occupied binding sites is 99% of the maximum bound CBM3a concentration at the end of reaction, $t_{(0.99)}$, was determined by fitting different concentrations of CBM3a against reaction time using the high resolution AFM images and the single-molecule kinetics equations. Based on the experimental data and kinetics calculations, the minimal effective initial CBM3a concentration was estimated to be 5.1 × $10^{-7}$ M at 287 min reaction time. This study provides an in-depth understanding of the binding mechanism of CBM with crystalline cellulose at single molecule level.

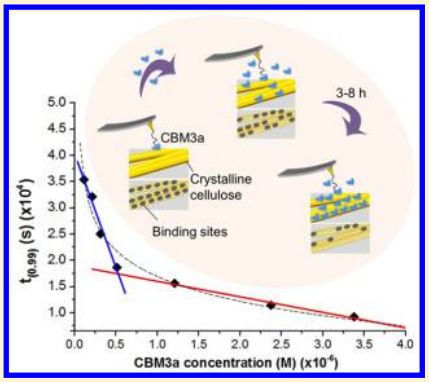


## INTRODUCTION

Lignocellulosic biomass (mainly plant cell walls) is a renewable source for biofuel production by enzymatic hydrolysis.[1,2] This procedure is greatly hindered by the natural complexity of the plant cell wall structure and composition. The closely packed cellulose chains are stabilized by hydrogen bonding to form a tight, regular array which hinders many of the glycosidic bonds from enzymatic attack. The carbohydrate-degrading enzymes are mainly composed of two domains with specific functions. One can specifically binding to carbohydrate surface, named carbohydrate-binding domain (CBD). The other is called catalytic domain[3] and is connected to the CBD by a short peptide linker. The CBD, or cellulose-binding modules (CBM), have been grouped into several families sharing the same basic structure and the same chemical reaction mechanism.[4] Some studies found that the removal of CBM could lead to a decrease of about 50−80% of the efficiency of cellulases on insoluble substrates.[5−7] These results indicated a direct correlation between the efficiency of cellulose degradation and enzyme binding. It has long been a great challenge to improve the efficiency of enzymatic hydrolysis, as little is known about the plant cell wall structural changes and the mechanism of the enzyme−cellulose interactions. Therefore, a more profound understanding of this process, especially at single-molecule level, is essential to the enzymatic biomass conversion and ultimately improves bioethanol production.[8,9]

As the beginning step of enzymatic hydrolysis of cellulose, the efficiency and affinity of CBM binding to plant cell walls can directly influence the degradation process. The CBM has been proposed to be responsible for the apparently irreversible binding, rather than the catalytic domain.[10,11] The CBM binding can guide the movement of intact cellulase molecules on the cellulose surface, the binding equilibrium is therefore of great importance for understanding hydrolysis process. The adsorption of CBMs is therefore required to be fully understood and well-controlled.[12] Measuring the single molecular CBM−cellulose interaction may provide a better understanding of the enzyme−cellulose interaction mechanism at single molecule level.

In the past decades, bulk experimental measurements quantitatively revealed a wide range of affinities of different CBMs binding to various cellulose substrates under a series of temperatures.[13−18] In 1996, Linder and Teeri studied the kinetics of binding of the CBM from *Trichoderma reesei* cellobiohydrolase I on microcrystalline cellulose based on binding isotherm data.[12] In this work, free CBM molecules (100 μL, 20 μM) were incubated with the same volume of bacterial microcrystalline cellulose (2 mg/mL) for 3 h. Binding affinity of the CBM was found to increase at lower temperatures. The exchange rate measured for the CBM−cellulose interaction compared well with the hydrolysis rate of cellobiohydrolase I with $k_{off}$ = 0.012 ± 0.0025 $s^{-1}$ at 22 °C.

**Received:** March 31, 2014
**Revised:** May 29, 2014
**Published:** May 30, 2014

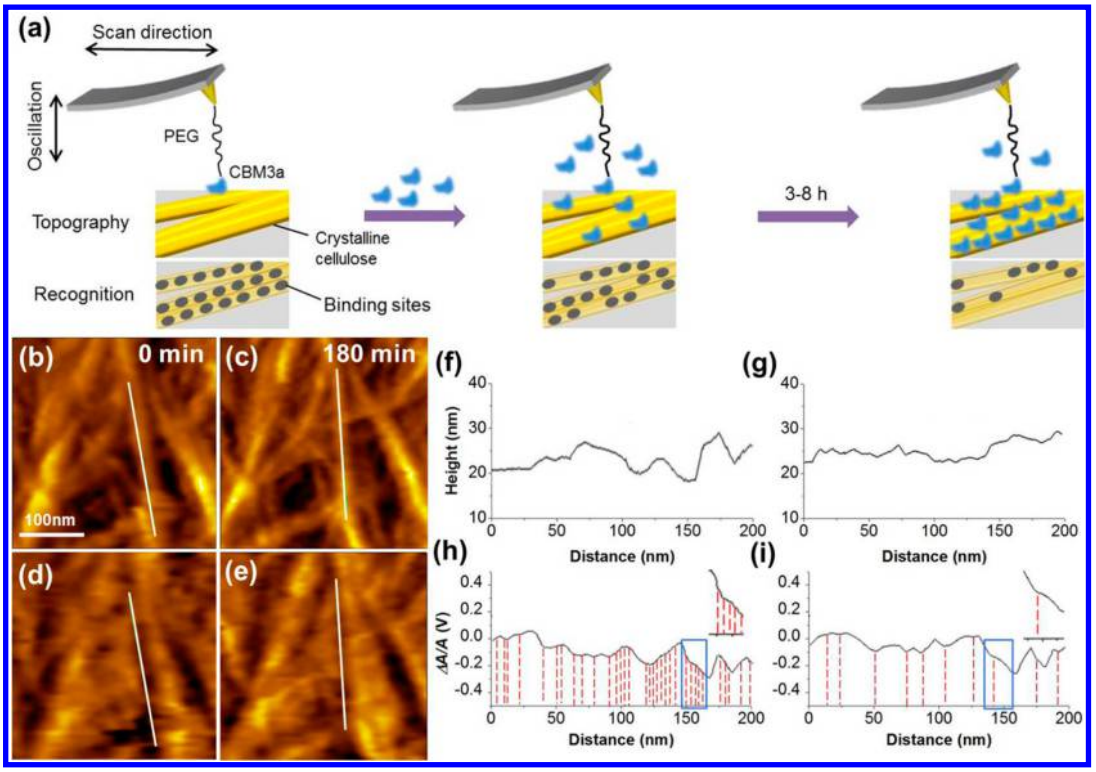


**Figure 1.** Schematics and AFM images of CBM3a binding to crystalline cellulose. (a) Schematics of the blocking of binding sites after injection of free CBM3a molecules; (b,c) Topography and (d,e) recognition images of crystalline cellulose fibril before (0 min) and after (180 min) presence of free CBM molecules (3.38 $\mu$M). The white lines label the topography (f,g) and recognition (h,i) cross-section of a single cellulose fibril. The red, dashed lines highlighted the individual binding sites before and after the blocking by free CBM molecules. The blue boxes indicate the differences of binding sites at 0 and 180 min on a certain location of that cellulose fibril.

McLean and co-workers extended the CBM species and cellulose substrates in 2002 to identify the specificities of different CBMs to different cellulose structures by competition isotherms and fluorescent labeling.[19] The adsorption isotherms were obtained by incubating 2−20 $\mu$M of competing fluorescence-labeled CBM species with cellulose substrates (1 mg/mL) for 3 h at 4 °C. The surface and solution concentrations of each CBM were monitored as a function of time and composition. A very fine binding specificity of cellulose-specific CBMs was determined down to the resolution of cellulose microstructures. This research provided a comprehensive understanding of how an enormous number of CBM molecules from different enzyme species bound to the carbohydrate substrates competitively and the specificity of each CBM was quantitatively determined. However, the complicated labeling procedure and averaged kinetic values made the measurement of binding efficiency down to the single CBM molecule impossible.

To better understand the binding process and efficiency of CBM binding, direct observation and measurement at single molecule level are needed to study the binding behavior of a single CBM molecule. An accurate measurement of binding efficiency and surface distribution of CBM bound to cellulose can provide very important information about the minimum concentration as well as reaction time for an optimal enzymatic hydrolysis process. Among the single molecule techniques, atomic force microscopy (AFM) has the advantages of imaging the sample surface with ultrahigh resolution, down to the single molecule and atomic level. AFM has already been widely used to directly visualize the surface structure of plant cell walls with nanometer resolution.[20−22] The morphology and surface roughness of the plant cell wall were precisely determined. Recently, AFM recognition imaging was combined with the dynamic force measurements to map the substrate components and measure the intermolecular forces using functionalized AFM tips.[23] In our previous work, AFM recognition imaging and single molecule dynamic force spectroscopy (SMDFS) have been applied to map the natural and pretreated plant cell wall surface and study the affinity between noncatalytic family 3 carbohydrate-binding modules (CBM3a) and crystalline cellulose.[24,25] The bottom of the CBM3a molecule consists some conserved surface residues, including five amino acid residues (Trp118, Arg112, Asp56, His57, and Tyr67), which form a planar and hydrophobic strip. Based on biochemistry study, this flat region will specifically interact with crystalline cellulose.[26] Therefore, CBM3a was chosen as the probe for the specific recognition of crystalline cellulose. The crystalline cellulose exposed on the cell wall surface before and after pretreatments was specifically recognized and its surface coverage changes were quantified.[27]

In this work, we studied the binding process of the CBM−cellulose interaction on extracted crystalline cellulose of poplar monitored by AFM topography and recognition images. CBM3a molecules (derived from *Clostridium thermocellum* Scaffoldin CipA) were used for both AFM tip functionalization and free CBM molecule binding under a series of concentrations. We also observed the distribution of bound CBMs on cellulose sample surfaces and determined the binding kinetics by a single-molecule kinetics model, which is based on counting the surface concentrations of CBM3a−cellulose complexes along the reaction time. Consequently, a minimal


dx.doi.org/10.1021/jp503185n | J. Phys. Chem. B 2014, 118, 6714−6720

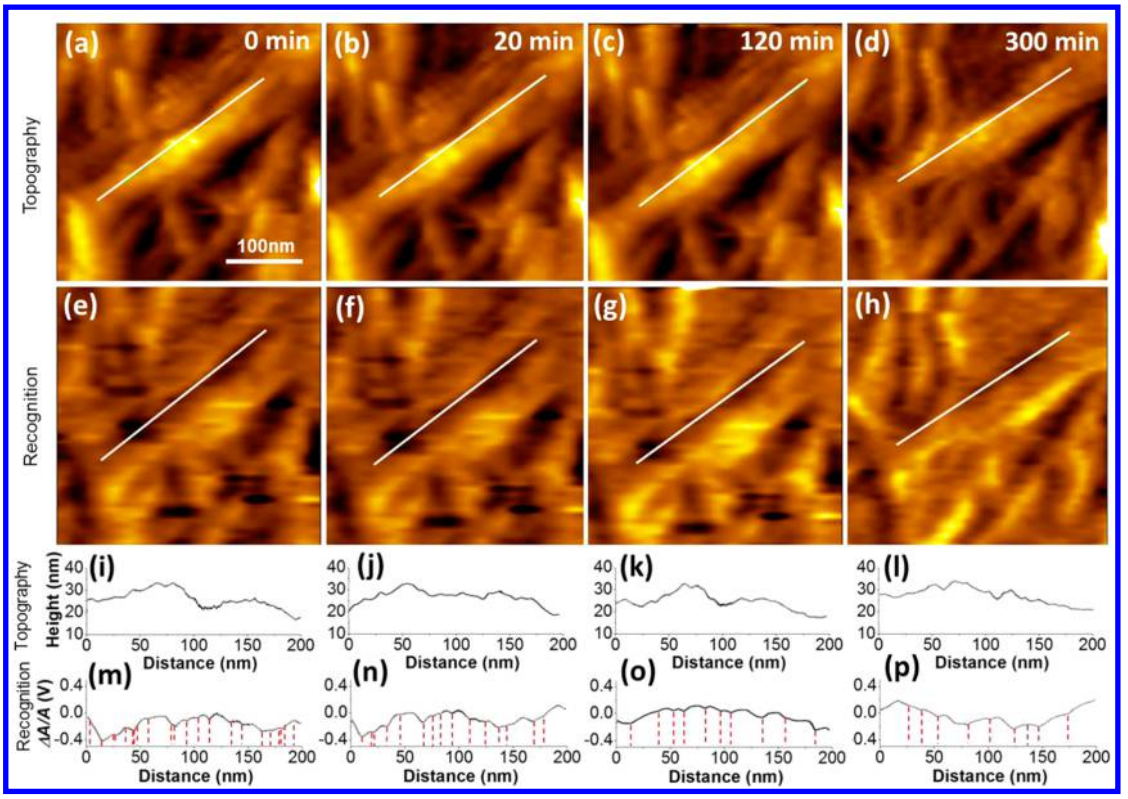


**Figure 2.** Timeline of CBM3a binding to crystalline cellulose: (a–d) topography images; (e–h) recognition images; (i–l) cross sections of topography images along the white lines; (m–p) cross sections of recognition images along the white lines. Some representative binding sites are labeled with red, dashed lines.

effective initial concentration of CBM3a was determined at a comparatively short reaction time using this kinetics model.

## EXPERIMENTAL METHODS

**Preparation of Recombinant CBM3a and AFM Tip Functionalization.** The recombinant CBM3a was provided by Complex Carbohydrate Research Center, University of Georgia as introduced previously.[24] The AFM tips (CS-25 silicon) with the nominal spring constant of 0.1 N/m were purchased from Nanoscience Instruments, Phoenix, AZ. The CBM3a-AFM tip functionalization procedure has been described in a previous publication.[24]

**Preparation of Extracted Plant Cell Wall Cellulose and AFM Sample.** The extraction of crystalline cellulose fibrils followed a widely used procedure and the details were depicted in our previous work.[25,28] To prepare the AFM sample for recognition imaging and binding site calculation, the extracted poplar suspension (0.1 wt %, 20 $\mu$L) was dropped onto the cleaned glass surface. After 20 min, the glass surface was washed by 200 $\mu$L purified water five times to remove extra cellulose that had weak adsorption to glass. Finally, the air-dried glass chip was fixed into an AFM flow cell[29] and then filled with 0.4 mL Tris-Cl buffer (10 mM Tris-Cl and 150 mM NaCl, pH = 7.5) for recognition imaging and binding site calculation.

**AFM Experimental Settings.** The PicoPlus system combined with an Agilent 5500 Controller was used in this work. An Agilent multipurpose AFM scanner was used to obtain images in an area as large as 10 $\mu$m by 10 $\mu$m. All the images were taken under Top magnetic AC (TopMAC) mode with a PicoTREC controller (Agilent Technologies, Santa Clara, CA). The whole system was enclosed by a PicoPlus Isolation Chamber to be shielded from environmental interference. After obtaining repeatable AFM images of extracted crystalline cellulose within the same scanned area, the CBM3a solution in 100 $\mu$L Tris-Cl buffer was gently injected into the flow cell. The CBM3a concentrations used in this work were 3.38 $\mu$M, 2.37 $\mu$M, 1.20 $\mu$M, 0.5 $\mu$M, 0.3 $\mu$M, 0.2 $\mu$M, and 0.1 $\mu$M. The binding process of CBM3a onto crystalline cellulose was then monitored in the following 3–8 h.

**Binding Site Calculation by AFM Recognition Imaging.** Under each CBM3a concentration, the binding experiment was repeated 3 times. The binding sites were calculated in a 300 nm × 300 nm scanned area, and 5 randomly selected locations on the sample surface were used to obtain the images with the same scan size in order to obtain average results. The functionalized AFM tip was set at a scanning speed of 6 $\mu$m/s. AFM recognition images have been used to calculated the recognition area percentage in our previous work.[25,27] To study the kinetics of the CBM3a binding process, the numbers (or concentrations) of available binding sites on the cellulose sample surface were counted from individual binding site, which was estimated as 5 nm in width with 5–8 nm interval along a single crystalline cellulose fibril.[24] Both the total binding sites at the beginning of the reaction and the unoccupied binding sites after a certain reaction time (which were converted into the numbers of the formed CBM–cellulose complex) were calculated from the AFM images with 300 nm × 300 nm scanned area.

## RESULTS AND DISCUSSION

Figure 1 shows the schematics and real-time AFM images of CBM3a binding to crystalline cellulose. As shown in Figure 1a, the CBM3a molecule functionalized on the AFM tip was induced to interact with the crystalline cellulose on substrate


dx.doi.org/10.1021/jp503185n | J. Phys. Chem. B 2014, 118, 6714–6720

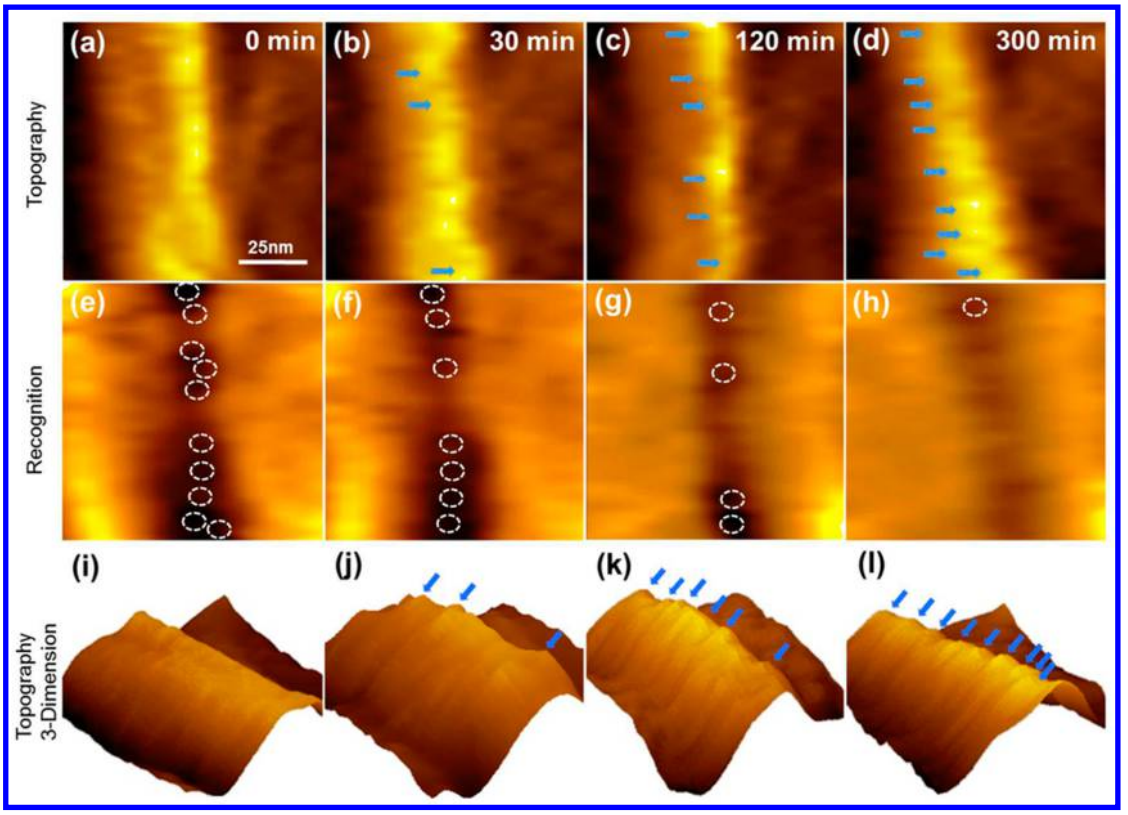


**Figure 3.** AFM topography (a–d), recognition (e–h), and 3D (i–l) images of CBM3a–cellulose binding at a smaller scale. The blue arrows in (b–d) and (j–l) indicate the regularly aligned CBM3a molecules binding on a crystalline cellulose fibril from 0 to 300 min. The binding sites are labeled by white, dashed circles.

during scanning. A series of recognition signals could be generated at the supposed binding sites along each crystalline cellulose fibril. The binding kinetics study was based on the initial concentrations of free CBM3a, the number of estimated available or initial binding sites on cellulose surface at the beginning of reaction, and the time-dependent formation of CBM-cellulose complex along the binding reaction course (Figure 1). The number of estimated binding sites was defined as the total number of binding sites located on the entire crystalline cellulose sample surface (300 nm × 300 nm scanned area). The interval between two adjacent binding sites was measured to be 5 to 8 nm (Figure 1h,i).[24,30] After injecting the CBM3a solution, the binding sites were gradually blocked by the free CBM molecules in solution; therefore, the number of available binding sites decreased. When coverage of the CBM3a molecules on the crystalline cellulose surface became saturated, most binding sites were blocked. The number (or concentration) of the CBM3a-crystalline cellulose complexes could be calculated by subtracting the number (or concentration) of unblocked binding sites (Figure 1i) from the total number of estimated available (initial) binding sites (Figure 1h). Therefore, the number of bound CBM3a-crystalline cellulose complexes was estimated to be 15–20 along a 200 nm fibril.

The crystalline cellulose surface with and without CBM binding was illustrated by AFM topography (Figure 1b,c) and recognition (Figure 1d,e) images. A representative crystalline cellulose fibril of diameter 20–25 nm was labeled by a white line along the axis. The cross-section along the white line was analyzed to show the difference of the surface morphology before and after CBM binding (Figure 1f–i). Before injecting the CBM3a solution, the surface of cellulose was comparatively rough with numerous binding sites available, as labeled by red dashed lines with the intervals of 5–15 nm in Figure 1h. At 180 min after injection of 3.38 $\mu$M of CBM3a, more small features appeared on the surface of cellulose fibril, which were supposed to be individual CBM3a molecules aligning along the cellulose fibrils. Therefore, the number of binding sites greatly decreased (less red dashed lines in Figure 1i), indicating the blocking of binding sites by free CBM molecules. The blue boxes in Figure 1h,i highlight the details of the change in binding sites between 0 and 180 min within a distance of 200 nm on cellulose fibril surface. Based on the observation of 15 crystalline cellulose fibrils, the average blockage ratio of the binding sites at 180 min was around 70–80% under this relatively high CBM concentration of 3.38 $\mu$M.

To reveal the details of the CBM binding process and the changes of cellulose surface morphology along the reaction time, a series of AFM topography and recognition images were collected with the initial CBM3a concentration of 0.2 $\mu$M, as an example. Figure 2 shows the images obtained at 0, 30, 120, and 300 min after injection of CBM3a solution. The cellulose surface morphology and the change of the binding sites were also revealed by cross-section analysis.

With the presence of CBM3a molecules, the surface of each crystalline cellulose fibril was gradually covered by CBM (Figure 2a–d). Simultaneously, more and more small features appeared along the cellulose fibril (Figure 2a–d). About 20 small "bumps" with diameter of ~5 nm were observed at 300 min along the fibril labeled by the white line, suggesting the regular alignment of CBM3a molecules (Figure 2i–l). Besides, the number of representative binding sites decreased from about 22 to 9 after 300 min reaction (Figure 2e–h and m–p),


dx.doi.org/10.1021/jp503185n | J. Phys. Chem. B 2014, 118, 6714–6720

indicating a weaker and nonspecific interaction between the CBM3a on the AFM tip and cellulose due to blocking of binding sites. Different from the results with the higher CBM concentration, the average blockage of binding sites reduced to 60−70% after saturated binding at 300 min under this lower concentration of CBMs.

Different from bulk experiments, we were able to directly observe the time-dependent alignment of individual CBM3a molecule along a single cellulose fibril at a smaller scale in AFM images (Figure 3). In topography images (Figure 3a−d), the morphology of the cellulose fibril kept changing and a highly regular pattern was finally observed along the fibril after 300 min, indicating the binding of increasing number of CBM molecules onto cellulose as indicated by the blue arrows. The recognition images (Figure 3e−h) showed a clearer trend of decreasing number of binding sites (as highlighted by the white dashed circles) due to the surface coverage of free CBM molecules.

The 3D images (Figure 3i−l) also provided the binding and alignment details of individual CBM molecule along cellulose fibril. After 120 min reaction, the CBM molecules on cellulose fibril began to show a regular pattern until the formation of a well-arranged alignment of nine "bumps" at 300 min (indicated by blue arrows in Figure 3b−d and j−l). Notably, the changes of the surface morphology and binding sites were significant during the first 120 min, but ones between 120 and 300 min were not pronounced. This difference implied that the CBM−cellulose binding happened faster in the first 1 to 2 h then slowed down until saturation. The same situation was also found in Figure 2k,l,o,p). The above observations provided important information on the binding behavior of CBM3a molecule. The binding efficiencies of CBM at different stages of time could lead to a more profound insight into the enzymatic hydrolysis process.

To quantitatively determine the binding process of CBM3a to cellulose, we also studied the reaction kinetics of CBM3a−cellulose interaction. The CBM3a binding reaction mechanism was based on a 1:1 single-molecule surface reaction model for the CBM3a and cellulose molecules. The CBM3a−cellulose interaction process can be expressed as follows:[31]

$$\mathrm{CBM3}a(M) + \mathrm{cellulose}(C) \left\langle \frac{k_{on}}{k_{off}} \right\rangle \mathrm{binding\ complex}(MC) \tag{1}$$

Here, $M$ is the concentration of injected CBM3a molecules; $C$ is the concentration of estimated initial binding sites on the cellulose surface; $MC$ is the concentration of CBM3a−cellulose binding complex at time $t$ on the sample surface. The calculations of $C$ and $MC$ were described in detail in SI Section S1 (Table S1). The initial concentration of CBM3a ($M_0$) was considered constant during the entire reaction course if excess of CBM3a molecules were added, compared to the relatively small concentration of cellulose ($C_0$) on the substrate surface.

After the estimated binding sites on cellulose in the scanned area were blocked by CBM3a molecules toward a saturation state, $MC(t)$ became a constant value $MC(\infty)$ (eq S1 and S2, SI Section S2). With the dissociate constant or off-rate $k_{off}$ estimated from the Bell's model of single-molecule unbinding force measurements,[32] the on-rate $k_{on}$ could also be determined from the relationship below (eq 2):

$$k_{on} = \frac{MC(\infty)k_{off}}{M_0[C_0 - MC(\infty)]} \tag{2}$$

Here, both the initial binding sites on cellulose molecules $C_0$ and the final binding complex $MC(\infty)$ were counted based on the AFM images. With $k_{off}$ value estimated from single-molecule unbinding force measurements,[25] the dissociation constant $k_d$ value was also calculated from the $k_{on}$ and $k_{off}$ (eq 3)

$$k_d = \frac{k_{off}}{k_{on}} \tag{3}$$

To better understand the specific process of CBM3a−cellulose interactions, seven different $M_0$ values (3.38 $\mu$M, 2.37 $\mu$M, 1.20 $\mu$M, 0.5 $\mu$M, 0.3 $\mu$M, 0.2 $\mu$M, and 0.1 $\mu$M) were used to obtain the real-time reaction curve. The fitting curves based on SI eq S2 were compared with their corresponding experimental data points (Figure 4). Here, the CBM3a concentrations were converted from the numbers of molecules counted in each AFM image along reaction time $t$. The saturation time $t_{(0.99)}$ was defined as the reaction time when the concentration of occupied binding sites is 99% of the maximum bound CBM3a concentration at the end of reaction (see the fitting curves in Figure 4). The value of $t_{(0.99)}$ at each concentration was calculated from its corresponding fitting curve, and highlighted as cross marks on the fitting curve of each $M_0$ concentration in Figure 4. The $k_d$ values also depended on the $M_0$ concentrations. When $M_0$ increased, both $MC(\infty)$ and $k_d$ increased in the binding process (Table S2, SI Section S3).

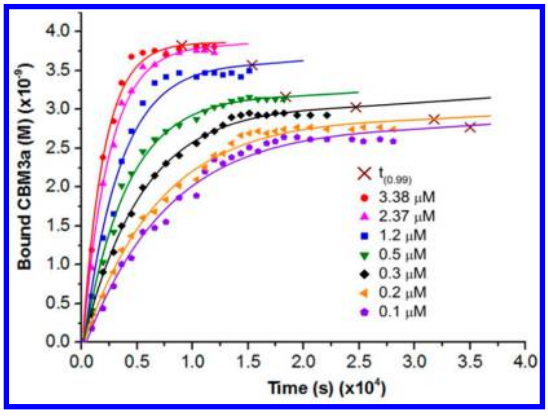


**Figure 4.** CBM3a against reaction time plots for different initial concentrations of CBM3a ($M_0$). $t_{(0.99)}$ is the saturation time when the concentration of occupied binding sites is 99% of the maximum bound CBM3a concentration at the end of reaction.

Both $M_0$ and $t$ showed the exponential relationships with the binding complex concentration $MC$ (eq S3, SI Section S2). Therefore, the relationship between $M_0$ and $t$ can be expressed as

$$t_{(0.99)} = \frac{\ln[C_0 - MC_{(0.99)}]}{-k_{on}M_0} \tag{4}$$

Here, $MC_{(0.99)}$ represents the saturation binding complex concentration at saturation time $t_{(0.99)}$. The plots of $t_{(0.99)}$ against $M_0$ are shown below. The saturation time significantly decreased when initial CBM3a concentration increased. According to eq 4, the initial CBM3a concentration $M_0$ and saturation time $t_{(0.99)}$ had a simple reciprocal relationship if the


dx.doi.org/10.1021/jp503185n | J. Phys. Chem. B 2014, 118, 6714−6720

change of saturation complex concentration, the *MC* value at $t_{(0.99)}$, could be neglected.

According to the work of Lee et al., the values of $k_{off}$, $k_{on}$, and $k_d$ obtained from the force spectroscopy approach differed from those obtained by a best fit of the data.[31] The distribution of free molecules was not expected to be homogeneous due to nonideal mixing of the injected solution. Therefore, the binding rate was assumed to lag behind the estimation in SI eq S2 under an ideal-mixing condition. This was also confirmed by SI eq S2 with the $k_{off}$ determined from force spectroscopy. Thereby, the binding kinetics could be determined more realistically using force spectroscopy in real experiments.

Figure 5 showed the plot of $t_{(0.99)}$ against $M_0$ and the trend of these data points was very close to a reciprocal relationship.

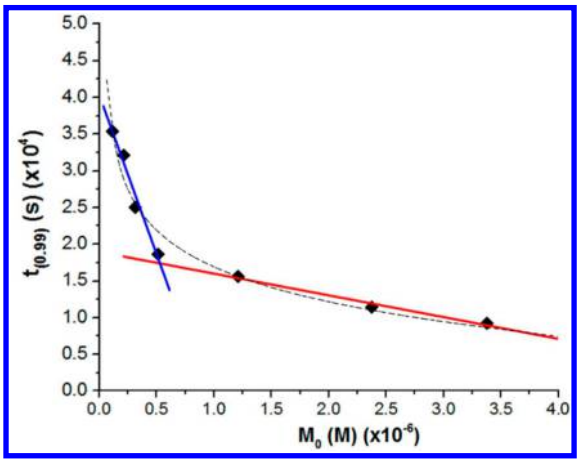


**Figure 5.** Plot of $t_{(0.99)}$ against a series of $M_0$. Data points determined by low $M_0$ and high $t_{(0.99)}$ are fitted by the blue line and data points determined by high $M_0$ and low $t_{(0.99)}$ are fitted by the red line. The trend of the changes of $t_{(0.99)}$ is guided by the black, dashed line. The point near intersection indicates the minimal effective initial concentration of $M_0$ (around $5.1 \times 10^{-7}$ M).

However, when $M_0$ decreased in the experiments, the value of saturation complex concentration (marked as a brown cross for each $M_0$ value in Figure 4) gradually decreased. Therefore, the saturation time $t_{(0.99)}$ was determined by both initial CBM3a concentration $M_0$ and measured complex concentration *MC* $t_{(0.99)}$. Strictly speaking, the relationship between $t_{(0.99)}$ and $M_0$ was more complex than a highly simplified reciprocal fitting curve.

In the experimental analysis, we aimed to obtain a minimal effective initial CBM3a concentration $M_0$ so that the binding reaction could reach saturation with a reasonable $t_{(0.99)}$. Here, linear fittings were used for the four data points in the left part and three data points in the right part of Figure 5. The intersection of these two fitting lines showed the minimal effective initial CBM3a concentration and its corresponding saturation time $t_{(0.99)}$. Based on this estimation, the initial CBM3a concentration should be $5.1 \times 10^{-7}$ M and the saturation time will be 17200 s or 287 min. If the purpose was to obtain a shorter saturation time, further increasing the CBM3a initial concentration would not be efficient any more. On the other hand, the CBM3a initial concentrations lower than $5.1 \times 10^{-7}$ M would dramatically increase the reaction time to reach binding saturation on the cellulose surface. The $5.1 \times 10^{-7}$ M should be an economic value for the CBM3a–cellulose surface binding reaction.

Other literature reported the reaction times of the CBM3a–cellulose interaction with various criteria and methods.[33,34] For instance, Goldstein and co-workers reported that a plateau value of the 1.2 $\mu$M complex was attained by 60 min with 2 $\mu$M CBM incubated with 1 mg/mL Avicel.[14] Besides, the measured complex concentration dropped to around half of the maximum value after prolonged incubation of 18 h. This was assumed to be caused by gradual denaturation of the CBMs or by disrupted cellulose surface during nonhydrolytic processes according to Din et al.[35] Our single-molecule measurements provided important information about the reaction process as well as time at the nanometer scale. It is well known that the binding kinetics can differ widely among cellulose sample preparations, surface immobilizations, reaction temperatures, and so forth. Thus, the very close agreement between bulk experiment and single molecule measurement was not expected in this study. In our work, we used small CBM molecules to study only the binding process and kinetics of CBM–cellulose interaction. When a larger enzyme molecule is used, a different and more complex hydrolysis process is supposed to be observed with different binding site distribution and changes of counts over a time course.

## CONCLUSIONS

In this work, the binding process of CBM3a molecules to crystalline cellulose fibrils was studied by AFM topography and recognition images. The free CBM3a molecules of different concentrations were observed to bind to crystalline cellulose efficiently and regularly, especially in the first 120 min. Single-molecule kinetics revealed the detailed relationships among the real-time CBM3a concentration on cellulose surface, reaction time, and initial CBM3a concentration in solution. The saturation time when the concentration of occupied binding sites is 99% of the maximum bound CBM3a concentration, $t_{(0.99)}$, was determined by the AFM recognition images and kinetic model we used in this study. The minimal effective initial CBM3a concentration was found to be $5.1 \times 10^{-7}$ M when the reaction time and initial CBM3a concentration were considered as critical conditions in the experiments. The single-molecule kinetics used in this study was based on large amounts of AFM experimental results and could guide the future experiments on similar reaction systems.

## ASSOCIATED CONTENT

### Supporting Information

Calculation of numbers of initial binding sites and CBM-cellulose complexes in a 150 nm × 150 nm scanned area; deviations of kinetic parameters; summary of the $k_{on}$ and $k_d$ values based on different initial CBM3a concentrations. This material is available free of charge via the Internet at http://pubs.acs.org.

## AUTHOR INFORMATION

### Corresponding Author

*Tel: (706)-542-0502. Fax: (706)-542-8806. E-mail: bxu@engr.uga.edu.

### Notes

The authors declare no competing financial interest.

## ACKNOWLEDGMENTS

Financial support of this research was provided by the National Science Foundation (ECCS 1231967, CBET 1139057).

## REFERENCES


(1) Jordan, D. B.; Bowman, M. J.; Braker, J. D.; Dien, B. S.; Hector, R. E.; Lee, C. C.; Mertens, J. A.; Wagschal, K. Plant Cell Walls to Ethanol. *Biochem. J.* **2012**, *442*, 241−252.

(2) Ding, S. Y.; Liu, Y. S.; Zeng, Y. N.; Himmel, M. E.; Baker, J. O.; Bayer, E. A. How Does Plant Cell Wall Nanoscale Architecture Correlate with Enzymatic Digestibility? *Science* **2012**, *338*, 1055−1060.

(3) Gilbert, H. J. The Biochemistry and Structural Biology of Plant Cell Wall Deconstruction. *Plant Physiol.* **2010**, *153*, 444−455.

(4) Shoseyov, O.; Shani, Z.; Levy, I. Carbohydrate Binding Modules: Biochemical Properties and Novel Applications. *Microbiol. Mol. Biol. Rev.* **2006**, *70*, 283−295.

(5) Klyosov, A. A. Trends in Biochemistry and Enzymology of Cellulose Degradation. *Biochemistry* **1990**, *29*, 10577−10585.

(6) Tomme, P.; Vantilbeurgh, H.; Pettersson, G.; Vandamme, J.; Vandekerckhove, J.; Knowles, J.; Teeri, T.; Claeyssens, M. Studies of the Cellulolytic System of *Trichoderma Reesei* QM 9414. Analysis of Domain Function in two Cellobiohydrolases by Limited Proteolysis. *Eur. J. Biochem.* **1988**, *170*, 575−581.

(7) Gilkes, N. R.; Jervis, E.; Henrissat, B.; Tekant, B.; Miller, R. C., Jr.; Warren, R. A. J.; Kilburn, D. G. The Adsorption of a Bacterial Cellulase and Its Two Isolated Domains to Crystalline Cellulose. *J. Biol. Chem.* **1992**, *267*, 6743−6749.

(8) Smith, L. G. Plant Cell Division: Building Walls in the Right Places. *Nat. Rev. Mol. Cell Biol.* **2001**, *2*, 33−39.

(9) Mccann, M. C.; Wells, B.; Roberts, K. Direct Visualization of Cross-Links in the Primary Plant Cell Wall. *J. Cell Sci.* **1990**, *96*, 323−334.

(10) Nidetzky, B.; Steiner, W.; Claeyssens, M. Cellulose Hydrolysis by the Cellulases from *Trichoderma Reesei*: Adsorptions of Two Cellobiohydrolases, Two Endocellulases and Their Core Proteins on Filter Paper and Their Relation to Hydrolysis. *Biochem. J.* **1994**, *303*, 817−823.

(11) Henrissat, B. Cellulases and Their Interaction with Cellulose. *Cellulose* **1994**, *1*, 169−196.

(12) Linder, M.; Teeri, T. T. The Cellulose-Binding Domain of the Major Cellobiohydrolase of Trichoderma Reesei Exhibits True Reversibility and a High Exchange Rate on Crystalline Cellulose. *Proc. Natl. Acad. Sci. U.S.A.* **1996**, *93*, 12251−12255.

(13) Tomme, P.; Boraston, A.; McLean, B.; Kormos, J.; Creagh, A. L.; Sturch, K.; Gilkes, N. R.; Haynes, C. A.; Warren, R. A. J.; Kilburn, D. G. Characterization and Affinity Applications of Cellulose-Binding Domains. *J. Chromatogr., B* **1998**, *715*, 283−296.

(14) Goldstein, M. A.; Takagi, M.; Hashida, S.; Shoseyov, O.; Doi, R. H.; Segel, I. H. Characterization of the Cellulose-Binding Domain of the *Clostridium Cellulovorans* Cellulose-Binding Protein A. *J. Bacteriol.* **1993**, *175*, 5762−5768.

(15) Georgelis, N.; Yennawar, N. H.; Cosgrove, D. J. Structural Basis for Entropy-Driven Cellulose Binding by a Type-A Cellulose-Binding Module (CBM) and Bacterial Expansin. *Proc. Natl. Acad. Sci. U.S.A.* **2012**, *109*, 14830−14835.

(16) Jervis, E. J.; Haynes, C. A.; Kilburn, D. G. Surface Diffusion of Cellulases and Their Isolated Binding Domains on Cellulose. *J. Biol. Chem.* **1997**, *272*, 24016−24023.

(17) Kurasin, M.; Valjamae, P. Processivity of Cellobiohydrolases Is Limited by the Substrate. *J. Biol. Chem.* **2011**, *286*, 169−177.

(18) Carrard, G.; Koivula, A.; Soderlund, H.; Beguin, P. Cellulose-Binding Domains Promote Hydrolysis of Different Sites on Crystalline Cellulose. *Proc. Natl. Acad. Sci. U.S.A.* **2000**, *97*, 10342−10347.

(19) McLean, B. W.; Boraston, A. B.; Brouwer, D.; Sanaie, N.; Fyfe, C. A.; Warren, R. A.; Kilburn, D. G.; Haynes, C. A. Carbohydrate-Binding Modules Recognize Fine Substructures of Cellulose. *J. Biol. Chem.* **2002**, *277*, 50245−50254.

(20) Liu, H.; Fu, S. Y.; Zhu, J. Y.; Li, H.; Zhan, H. Y. Visualization of Enzymatic Hydrolysis of Cellulose Using AFM Phase Imaging. *Enzyme. Microb. Technol.* **2009**, *45*, 274−281.

(21) Yan, L.; Li, W.; Yang, J.; Zhu, Q. Direct Visualization of Straw Cell Walls by AFM. *Macromol. Biosci.* **2004**, *4*, 112−118.

(22) Müller, D. J.; Dufrêne, Y. F. Atomic Force Microscopy As a Multifunctional Molecular Toolbox in Nanobiotechnology. *Nat. Nanotechnol.* **2008**, *3*, 261−269.

(23) Hinterdorfer, P.; Dufrêne, Y. F. Detection and Localization of Single Molecular Recognition Events Using Atomic Force Microscopy. *Nat. Methods* **2006**, *3*, 347−355.

(24) Zhang, M. M.; Wu, S. C.; Zhou, W.; Xu, B. Q. Imaging and Measuring Single-Molecule Interaction between a Carbohydrate-Binding Module and Natural Plant Cell Wall Cellulose. *J. Phys. Chem. B* **2012**, *116*, 9949−9956.

(25) Zhang, M. M.; Wang, B.; Xu, B. Q. Measurements of Single Molecular Affinity Interactions between Carbohydrate-Binding Modules and Crystalline Cellulose Fibrils. *Phys. Chem. Chem. Phys.* **2013**, *15*, 6508−6515.

(26) Tormo, J.; Lamed, R.; Chirino, A. J.; Morag, E.; Bayer, E. A.; Shoham, Y.; Steitz, T. A. Crystal Structure of a Bacterial Family-III Cellulose-Binding Domain: A General Mechanism for Attachment to Cellulose. *EMBO J.* **1996**, *15*, 5739−5751.

(27) Zhang, M. M.; Chen, G. J.; Kumar, R.; Xu, B. Q. Mapping out the Structural Changes of Natural and Pretreated Plant Cell Wall Surfaces by Atomic Force Microscopy Single Molecular Recognition Imaging. *Biotechnol. Biofuels* **2013**, *6*.

(28) Li, R. J.; Fei, J. M.; Cai, Y. R.; Li, Y. F.; Feng, J. Q.; Yao, J. M. Cellulose Whiskers Extracted from Mulberry: A Novel Biomass Production. *Carbohydr. Polym.* **2009**, *76*, 94−99.

(29) Ebner, A.; Kienberger, F.; Kada, G.; Stroh, C. M.; Geretschlager, M.; Kamruzzahan, A. S. M.; Wildling, L.; Johnson, W. T.; Ashcroft, B.; Nelson, J.; Lindsay, S. M.; Gruber, H. J.; Hinterdorfer, P. Localization of Single Avidin-Biotin Interactions Using Simultaneous Topography and Molecular Recognition Imaging. *ChemPhysChem* **2005**, *6*, 897−900.

(30) Ding, S. Y.; Xu, Q.; Ali, M. K.; Baker, J. O.; Bayer, E. A.; Barak, Y.; Lamed, R.; Sugiyama, J.; Rumbles, G.; Himmel, M. E. Versatile Derivatives of Carbohydrate-Binding Modules for Imaging of Complex Carbohydrates Approaching the Molecular Level of Resolution. *Biotechniques.* **2006**, *41*, 435−436 , 438, 440 passim..

(31) Lee, S.; Mandic, J.; Van Vliet, K. J. Chemomechanical Mapping of Ligand-Receptor Binding Kinetics on Cells. *Proc. Natl. Acad. Sci. U.S.A.* **2007**, *104*, 9609−9614.

(32) Bell, G. I. Models for the Specific Adhesion of Cells to Cells. *Science* **1978**, *200*, 618−627.

(33) Gill, J.; Rixon, J. E.; Bolam, D. N.; McQueen-Mason, S.; Simpson, P. J.; Williamson, M. P.; Hazlewood, G. P.; Gilbert, H. J. The type II and X Cellulose-Binding Domains of Pseudomonas Xylanase a Potentiate Catalytic Activity against Complex Substrates by a Common Mechanism. *Biochem. J.* **1999**, *342*, 473−480.

(34) Bolam, D. N.; Ciruela, A.; McQueen-Mason, S.; Simpson, P.; Williamson, M. P.; Rixon, J. E.; Boraston, A.; Hazlewood, G. P.; Gilbert, H. J. Pseudomonas Cellulose-Binding Domains Mediate Their Effects by Increasing Enzyme Substrate Proximity. *Biochem. J.* **1998**, *331*, 775−781.

(35) Din, N.; Gilkes, N. R.; Tekant, B.; Miller, R. C., Jr.; Warren, R. A. J.; Kilburn, D. G. Non-Hydrolytic Disruption of Cellulose Fibers by the Binding Domain of a Bacterial Cellulase. *Nat. Biotechnol.* **1991**, *9*, 1096−1099.